Volume 23
Number 2

December *2021*
(ISSN 1109-1606)

# Journal of

# APPLIED ELECTROMAGNETISM

JAE

Trans Black Sea Region Union of Applied Electromagnetism
BSUAE

**Institute of Communication and Computer Systems**

**Athens - GREECE**

**Volume 23** **December 2021**
**Number 2** **(ISSN 1109-1606)**

# JOURNAL
# OF
# APPLIED ELECTROMAGNETISM


**Institute of Communication and Computer Systems**

**Athens - GREECE**

**Volume 23** **Number 2**

**December 2021**

# TRANS BLACK SEA REGION UNION OF APPLIED ELECTROMAGNETISM (BSUAE)

## JOURNAL OF APPLIED ELECTROMAGNETISM

Institute of Communication and Computer Systems

Athens - GREECE

**Editor: Panayiotis Frangos (Greece),** pfrangos@central.ntua.gr

**Honorary Editor: Nikolaos K. Uzunoglu (Greece),** nuzu@central.ntua.gr

**Board of Associate Editors**

D. Dimitrov (Bulgaria), dcd@tu-sofia.bg
V. Dumbrava (Lithuania), vydum@ktu.lt
G. Georgiev (Bulgaria), gngeorgiev@yahoo.com
G. Matsopoulos (Greece), gmatso@esd.ece.ntua.gr

**Editorial Board**

ALBANIA
G. Bardhyf, bardhylgolemi@live.com
C. Pirro, p_cipo@yahoo.com

ARMENIA
H. Bagdasarian, hovik@seua.sci.am
H. Terzian, hterzian@seua.sci.am

BULGARIA
A. Antonov, asantonov@abv.bg
A. Lazarov, lazarov@bfu.bg
S. Savov, savovsv@yahoo.com

GEORGIA
R. Zaridze, rzaridze@laetsu.org

GERMANY
M. Georgieva – Grosse, mariana.georgieva-grosse@de.bosch.com

GREECE
H. Anastassiu, ANASTASIOU.Christos@haicorp.com
I. Avramopoulos, hav@mail.ntua.gr
G. Fikioris, gfiki@cc.ece.ntua.gr
J. Kanellopoulos, ikanell@cc.ece.ntua.gr
G. Karagiannidis, geokarag@auth.gr
G. Kliros, gsksma@hol.gr
T. Mathiopoulos, mathio@space.noa.gr
C. Moschovitis, harism@noc.ntua.gr
K. Nikita, knikita@cc.ece.ntua.gr

I. Ouranos, iouranos@central.ntua.gr
E. Papkelis, spapkel@central.ntua.gr
J. Sahalos, sahalos@auth.gr
M. Theologou, theolog@cs.ntua.gr
N. Triantafyllou, nitriant@central.ntua.gr
K. Ksystra, katksy@central.ntua.gr
A. Malamou, annamalamou@yahoo.gr
S. Bourgiotis, sbourgiotis@mail.ntua.gr

JORDAN
N. Dib, nihad@just.edu.jo

KAZAKSHTAN
S. Sautbekov, sautbek@mail.ru

LITHUANIA
L. Svilainis, linas.svilainis@ktu.lt

RUSSIA
M. Bakunov, bakunov@rf.unn.ru
A. Grigoriev, adgrigoriev@mail.ru

SERBIA
B. Reljin, ereljin@ubbg.etf.bg.ac.yu

SPAIN
E. Gago – Ribas, egr@tsc.uniovi.es
M. Gonzalez – Morales, gonmor@yllera.tel.uva.es

UNITED KINGDOM
G. Goussetis, G.Goussetis@hw.ac.uk

**Publishing Department**

N. Triantafyllou, nitriant@central.ntua.gr
K. Ksystra, katksy@central.ntua.gr
A. Malamou, annamalamou@yahoo.gr
S. Bourgiotis, sbourgiotis@mail.ntua.gr

# Journal of Applied Electromagnetism

## Copyright Form

**The undersigned I confirm that I agree the publication of the article**

**in the Journal of Applied Electromagnetism and the copyright to belong to Trans Black Sea Union of Applied Electromagnetism. I understand that I have the full right to reuse this manuscript for my own purposes.**

**Name:**

**Surname:**

**Address:**

**E-mail:**

**Signed:**

***Please send the previous form signed either by e-mail to pfrangos@central.ntua.gr , or by fax to the fax number: +30 210 772 2281, attention of Prof. P. Frangos.**

**Address**

Institute of Communication and Computer Systems,

National Technical University of Athens,

9, Iroon Polytechniou Str.,

157 73 Athens - GREECE

**Tel**: (+30) 210 772 3694

**Fax**: (+30) 210 772 2281, attention of Prof. P. Frangos

**e-mail**: pfrangos@central.ntua.gr

**Web site**: **http://jae.ece.ntua.gr**

**TRANS BLACK SEA REGION UNION OF APPLIED ELECTROMAGNETISM (BSUAE)**

**JOURNAL OF APPLIED ELECTROMAGNETISM (JAE)**

**Volume 23 Number 2 December 2021**

**CONTENTS**



*Novel closed-form expressions for auto- and cross-correlation functions are developed first for deterministic continuous signals presented by generalized Gauss-Hermite pulses (GHP). These set of functions is chosen because their special property: they are eigen-functions of the Fourier transform. Then complex electromagnetic signals based on mixture of these deterministic signals are developed. This analysis could be interesting for different areas: 1) analysis of ultra-wide band (UWB) antennas; 2) analysis of radar signals; 3) analysis of bio-electromagnetic signals.*



*Diffusion processes occur in many scientific areas; they are especially important in chemistry, biology and medicine. Most of the mathematical models that describe diffusion are nonlinear Partial Differential Equations, which do not have analytical solutions and numerical methods require large computing resources. There is a growing interest in the structures (fractal clusters) generated by diffusion processes, and the search for new models has intensified. The important method complementary to mathematical models is imitation modeling in which the space mobility of the particles of a substance is directly modeled.*

*There are two directions in such an approach: an imitation of random walks of particles; and cellular automata modeling. In this work, for the modeling of the fractal cluster growth on triangulated surfaces, we implement algorithms based on random walk. We use classical variants of Diffusion Limited Aggregation (DLA) and Reaction Limited Aggregation (RLA) models. It is shown that, in the framework of the classical Cluster Aggregation (CCA) model, fractal cluster on a triangulated surface cannot be correctly constructed without additional assumptions about the cluster restructuring.*

*The software is written in Python; it may be used by both researchers and students as a tool for the modeling of complex processes.*

**AN ANALYSIS OF UNCERTAINTY AND STATISTICS OF HIGH DYNAMIC RANGE ACOUSTIC SIGNALS (selected from CEMA'21 Conference)**



*A number of large dynamic range acoustic signals statistics has been presented based on continuous wavelet transform. Some typical examples from battlefield acoustics and from musical acoustics are considered. Therefore, a specialized platform and a measuring microphone with the required features are used in field experiments. The characteristic acoustic environment signature and background noise features for some concrete setup are described.*

*Possible directions for using these technics for signal statistics analysis for retrieving useful information, based on Shannon entropy, are outlined. The datasets consisting of the raw data and metadata from bell ringing and gunfire, and noise recordings are estimated. The wavelet transform was of particular importance here, as it provides both constant-bandwidth analysis that correlates with sound perception and optimal resolution. The discussed problems by means of continuous wavelet transform (CWT) and decomposition (or Shannon) entropy are approached. The results can be used in various areas of acoustics and electrodynamics.*

**REVISITING ENHANCED AIS DETECTION RANGE UNDER DUCTING (selected from CEMA'21 Conference)**



*This report studies the propagation of Automatic Identification System frequencies under various tropopheric ducting and sea surface conditions with the parabolic wave equation method. The aim is to examine the influence of sea surface roughness on the possibility to enlarge the AIS detection range under ducting.*

# CLOSED-FORM EXPRESSIONS FOR TIME-CORRELATIONS OF DETERMINISTIC SIGNALS PRESENTED BY GAUSS-HERMITE PULSES

Sava V. Savov*

*Department of Electrical Engineering, Technical University of Varna,
9010 Varna, Bulgaria

E-mail: sava.savov12@gmail.com

## Abstract

*Novel closed-form expressions for auto- and cross-correlation functions are developed first for deterministic continuous signals presented by generalized Gauss-Hermite pulses (GHP). These set of functions is chosen because their special property: they are eigen-functions of the Fourier transform. Then complex electromagnetic signals based on mixture of these deterministic signals are developed. This analysis could be interesting for different areas: 1) analysis of ultra-wide band (UWB) antennas; 2) analysis of radar signals; 3) analysis of bio-electromagnetic signals.*

**Index terms** – *Time-domain analysis, Gauss-Hermite electromagnetic pulses (EMP), Auto- and cross-correlation functions.*

## 1. INTRODUCTION AND PROBLEM FORMULATION

In this paper a set of *Fourier - Hermite pulses* (GHP) as a special class of *electromagnetic pulses* (EMP) are proposed and their correlation properties are explored. These pulses have special advantages that make them an important class of EMP. They are orthogonal functions. They are generalization of important class for the applications Gaussian pulses. Finally, they are eigen-functions of the important Fourier integral transform. In principle, every radar pulse could be expressed in term of series of these short GHP pulses. The obtained signals are well localized, have a high spectral efficiency and a robustness against synchronization errors, which is similar to the robustness of the common orthogonal trigonometric Fourier pulses. Based on discussed properties and initial results, the Fourier-Hermite signal set is found to be a promising candidate for

many areas of signal processing applications (including exploration of general EMP). In the analysis below novel analytical results are obtained for the *auto- and cross-correlations* between different members of the class of the GHP. Another positive result is that the last results are expressed in term of associated Laguerre pulses, that are also well tabulated an orthogonal set of functions.

GHP pulses can be used in different applications: eigenmodes in multi-mode optical fibers [1], Hermite functions find application in image processing [2], [3], optics [4], electroencephalograph (EEG) processing [5], ultra-wideband (UWB) pulseshaping [6], short-time pulse radar [7], and in multicarrier UWB-communications [8] - [10].

Auto-correlation functions of Hermite functions have first been addressed in 2003 [11]. Next, in 2003 also were derived cross-correlation functions for a generalized class of Hermite functions, called generalized Hermite wavelets, however they are presented by a single series [12]. The author noticed that his results *"strongly suggest that the correlation functions of generalized Hermite wavelets can also be represented by generalized Hermite wavelets".* As the Gaussian pulses is in fact the zeroth-order GHP, and the results of the operations on the zeroth-order GHP are well-established. We extend here the conventional Gaussian EMP and more general Gauss-Hermite pulses of an arbitrary order are used instead. As Hermite functions have several well-studied properties and often serve as an orthonormal signal basis, it is advantageous to express the results of mathematical operators in terms of Hermite functions. It allows for subsequent reuse of the same equations when multiple operations are performed consecutively [12], [13].

The GHP correlations are investigated in the recent papers [14], [15], however the final results there are presented in terms of complicated double series form. In this paper much more simple explicit expressions for auto- and correlations of the GHP pulses are developed in terms of well-known associated Laguerre functions.

## 2. THE ORTHOGONAL SET OF GAUSS-HERMITE PULSES (GHP)

The Generalized Gauss-Hermite (GHP) generalized functions consist the important for the applications *Gaussian distribution as a particular case* for (n = 0). By definition they are the following set of time-domain functions

$$\phi_n\,(t) = \; C_n \; e^{-t^2/2}\, H_n\;(t)\,, \tag{1}$$

where the coefficients $C_n = 1\,/\,\sqrt{2^n\; n!\;\sqrt{\pi}}$ and $H_n\,(t)$ are Hermite polynomials, order (n).

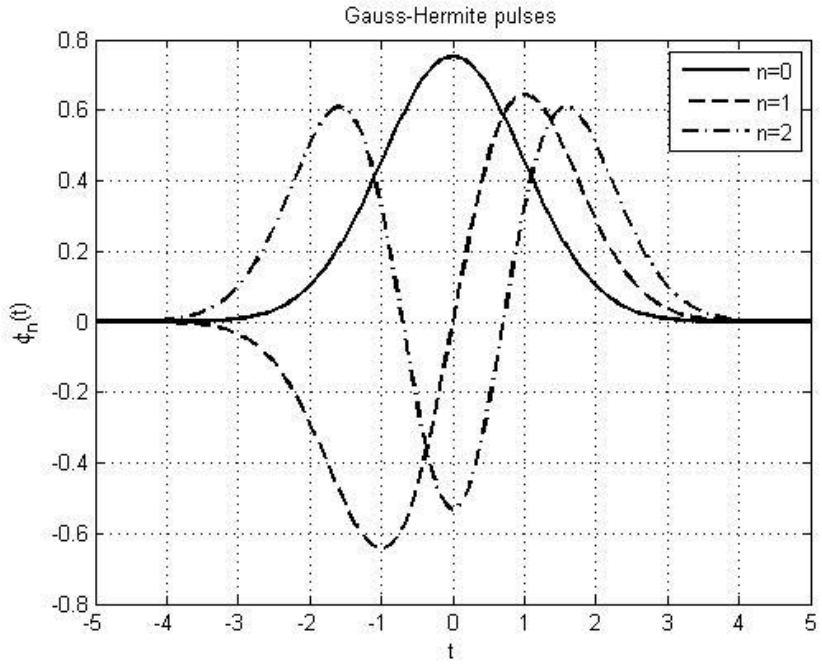


Figure 1. GHP for different indexes:
(n=0) - solid line; (n=1) – dashed line; (n=2) – dash-dotted line.

These coefficients are chosen in such way that the GHP become *orthonormal functions*, i.e.

$$\int_{-\infty}^{\infty} \phi_m\,(t)\;\phi_n\,(t)dt = \;\delta_{mn}\;\,, \tag{2}$$

where $\delta_{mn}$ are Kronecker symbols [15]. The first three functions (n=0; 1; 2) are shown in Fig.1. The pulses with n = even number are even functions, while these with n = odd number are odd functions. The lowest order GHP is just a Gaussian pulse function.

Next advantage of the GHP pulses is that they are *eigen-functions* of the infinite Fourier transform, because of the following property

$$\int_{-\infty}^{\infty} \phi_n\,(t)\,e^{j\omega t}dt = \;\sqrt{2\pi}\,j^n\;\phi_n\,(\omega) \tag{3}$$

Providing that the radar processes a general EMP $\{f(t)\}$, the last one can be presented in a series of GHP, or

$$f(t) = \;\sum_{n=0}^{\infty} b_n\;\phi_n\,(t) \tag{4}$$

where because of the orthogonality (2) the coefficients $\{b_n\}$ can be easily found by an integration

$$b_n = \int_{-\infty}^{\infty} f(t)\, \phi_n\ (t)dt\ . \tag{5}$$

Here we are interested in the properties of the auto- and cross-correlation functions of GHP and suitable novel analytic expressions will be developed below. It is shown how these two types of correlations can be extended for the case of general (deterministic or stochastic) EMP functions $\{f(t)\}$, defined by (4).

In some references two more similar convolution functions, called Wigner-distribution functions (WDF) and ambiguity functions (AF), are defined and suitable analytical series expressions for them are obtained [14], [15].

## 3. AUTO-CORRELTIONS OF GHP SET OF FUNCTIONS

By definition the auto-correlations of stationary deterministic/random processes with pdf-function presented by equation (1) can be found by the following integral

$$\rho_{nn}\,(\tau) = \ C_n^2\ \int_{-\infty}^{\infty} \phi_n\,(t)\ \phi_n\,(t+\ \tau)dt. \tag{6}$$

We introduce new integration variable by setting $t + \frac{\tau}{2} = \ \xi$ that transform this integral in the following form

$$\rho_{nn}\,(\tau) = \ C_n^2\ e^{-\tau^2\,/\,4} \int_{-\infty}^{\infty} H_n\,(\xi - \ \tau\ /2)\ H_n\,(\xi + \ \tau\ /2)d\xi. \tag{7}$$

Applying the reference [16] , setting: m = n, x = ξ, y = - τ/2, z = + τ/2, the following result is obtained for the auto-correlations

$$\rho_{nn}\,(\tau) = \ e^{-\tau^2\,/\,4}\ L_n^0\ (\tau^2\ /\ 2), \tag{8}$$

where $L_n^0\ (t)$ are Laguerre polynomials of order n.

The most widely used is the s.c. *envelope auto-correlations*, introduced by

$$\rho_{nn}^e\,(\tau) = \ |\rho_{nn}\,(\tau)|^2\ , \tag{9}$$

because of the fact that they are positive functions, or $\rho_{nn}^e\,(\tau) \geq 0$ for every time-interval $\tau$. The equations (9) and (6) lead to the following final result

$$\rho_{nn}^e\,(\tau) = \ e^{-\tau^2\,/\,2}\ |L_n^0\ (\tau^2\ /\ 2)|^2 \tag{10}$$

The first three autocorrelations (n = 0; n = 1; n = 2) are shown in Fig.2 for the case ($\tau > 0$ ). They are even-functions, so their behavior for ( $\tau < 0$ ) can be easily found. This means that they obey the following property

$$\rho_{nn}^{e}(-\tau) = \rho_{nn}^{e}(\tau). \tag{11}$$

As can be easily seen from Fig. 2, the number of the side-lobes of the auto-correlation function is equal to (n). Another observation is that the *width of the main lobe of the correlation function* (related to the correlation time interval) is decreasing with increasing of the order (n).

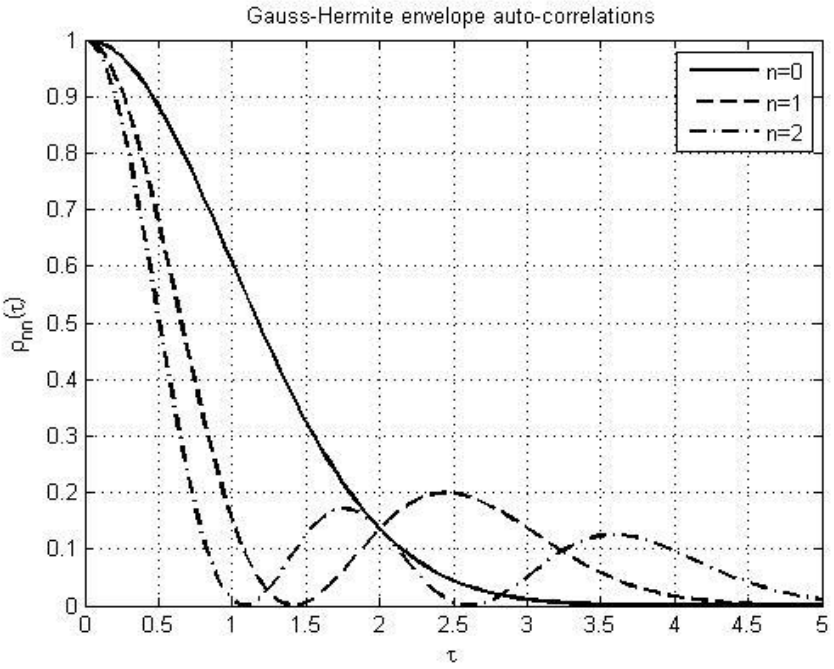


Figure 2. Auto-correlations of GHP:
(n=0) – solid line; (n=1) – dashed line; (n=2) – dash-dotted line.

## 4. CROSS-CORRELTIONS OF GHP SET OF FUNCTIONS

By definition the cross-correlations for two stationary random processes are a set of the following functions

$$\rho_{mn}(\tau) = C_m C_n \int_{-\infty}^{\infty} \phi_m(t)\, \phi_n(t+\tau) dt\,. \tag{12}$$

Applying the reference [16], setting: x = ξ, y = - τ/2, z = + τ/2, the following result for the cross-correlations is obtained

$$\rho_{mn}(\tau) = \sqrt{\frac{m!}{n!}} e^{-\tau^2/4} \ (\tau^2/2)^{(n-m)/2} L_m^{(n-m)/2}(\tau^2/2), \qquad (13)$$

where $L_m^n(t)$ are associated Laguerre – functions. From this equation the following final expression for the envelope cross-correlation function can be developed

$$\rho_{mn}^e(\tau) = \frac{m!}{n!} e^{-\tau^2/2} \ (\tau^2/2)^{n-m} \left| L_m^{(n-m)}(\tau^2/2) \right|^2 \ (m \le n) \qquad (14)$$

The first three cross-correlation functions (m = 0, n = 1); (m = 1, n = 2); (m = 0, n = 2) are shown in Fig.3. Obviously, the expression (10) is a special case of (14), when ( m = n ). From this expression is easily to prove that the envelope cross-correlations are also even functions,

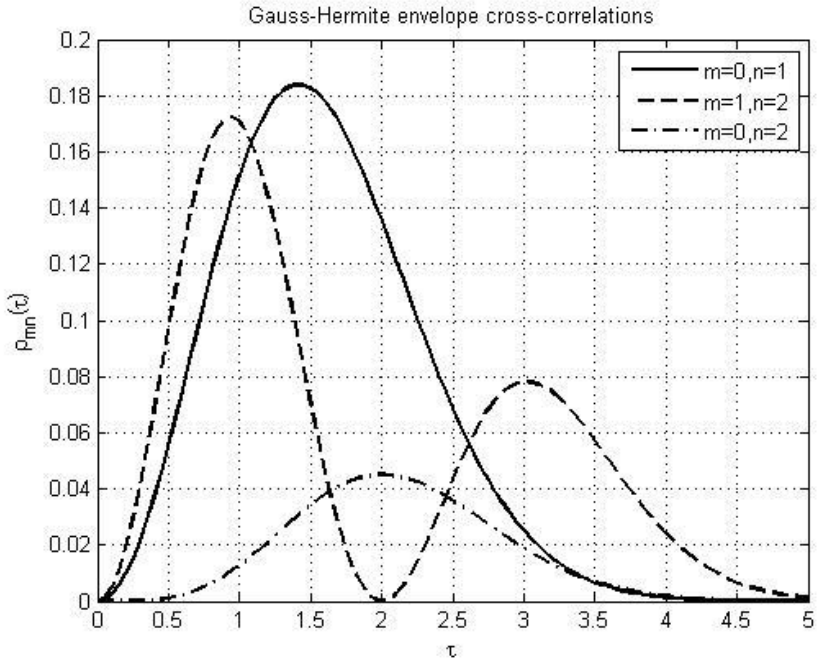


Figure 3. Cross-correlations of GHP:
(m=0, n=1) – solid line; (m=1, n=2) – dashed line; (m=0, n=2) – dashed-dotted line.

or

$$\rho_{mn}^e(-\tau) = \rho_{nm}^e(\tau) \qquad (15)$$

As it can be seen from Fig.3 the number of the maxima is related to the first index (m) and this number is (m+1) maxima. As it can be expected the *maximum values* of these cross-correlations is decreasing with increasing the distance from the main diagonal (see here the case m=0, n=2).

From Figs. 2 and 3 is visible, that the *correlation time* for all GHP is $T_c < 5$ , that proves the fact that GHP are well-localized EMP.

## 5. AUTO- AND CROSS- CORRELATIONS OF GENERAL ELECTROMAGNETIC PULSES (EMP)

Suppose now that we an arbitrary EMP f(t) is given by the series (4) in terms of well-known GHP $\phi_n\ (t)$ (n = 0, 1, 2, …,). The coefficients $\{b_n\}$ in this expression are found from equation (5) and they are assumed to be known. The correlation function $R\ (\tau)$ for these pulses (in case of a *stationary deterministic/random process*) can be defined by expression similar to (12), i.e.

$$R(\tau) = \int_{-\infty}^{\infty} f\ (t)\ f(t+\tau)\ . \tag{16}$$

Applying equation (4) yields to the following quadratic form

$$R\ (\tau) = \sum_{m=0}^{\infty} \sum_{n=0}^{\infty} b_m\ b_n\ \rho_{mn}\ (\tau). \tag{17}$$

This double series expression solves the problem with finding *the single time-correlation function* $R(\tau)$, provided the coefficients $\{b_n\}$ are known from (5) and the GHP correlation functions $\{\rho_{mn}\ (\tau)\}$ are known from (13). The envelope function of the EMP can be obtained from the expression

$$R^e(\tau) = |R\ (\tau)|^2 \tag{18}$$

## 4. CONCLUSION

In this paper an extension of the previous analytical expressions for the GHP pulses is developed. These novel expressions are much simpler and they provide more suitable procedure for numerical calculations of the time-correlations, than the algorithms proposed in [9] - [14], where single and double series are applied to obtain the correlations. Both auto- and cross-correlation functions are found in terms of well-tabulated Laguerre functions.

The obtained signals are well localized, have a high spectral efficiency and a robustness against synchronization errors, which is similar to the robustness of the common orthogonal trigonometric Fourier pulses. Based on discussed properties and initial results, a Fourier set of Gauss-Hermite signals (GHP) is found to be a promising candidate for many areas of signal processing applications (including exploration of general EMP).

The main analytical results obtained in this paper are simple explicit expressions in terms of Laguerre polynomials in the case of auto-correlations (10) and in the case of cross-correlations (14). The main numerical results easily derived in the paper by an application of these expressions are presented in Fig.2 and Fig.3. It can be easily seen that the correlation time ($T_c < 5$), which proves the fact that they are well-localized.

GHP pulses can be used in different applications: eigenmodes in multi-mode optical fibers [1], Hermite functions find application in image processing [2], [3], optics [4], electroencephalograph (EEG) processing [5], ultra-wideband (UWB) pulseshaping [6], wide-band radar [7] and as a basis for multicarrier UWB-communications [8] – [10].

**REFERENCES**

[1] M. Santarsiero, et al., "Evaluation of the modal structure of light beams composed of incoherent mixtures of Hermite-Gaussian modes,"Appl.Opt., vol. 38, no. 25, pp. 5272–5281, 1999.

[2] B. Martens, "The Hermite transform—Theory," IEEE Trans.Acoust., Speech, Signal Process., vol. 38, no. 9, pp. 1595–1606, 1990.

[3] J. B. Martens, "The Hermite transform—Applications," IEEE Trans.Acoust., Speech, Signal Process., vol. 38, no. 9, pp. 1607–1618, 1990.

[4] [H. M. Ozaktas et al., "Convolution, filtering, and multiplexing in fractional Fourier domains and their relation to chirp and wavelet transforms," J. Opt. Soc. Amer. A., vol. 11, no. 2, pp. 547–559, 1994.

[5] Y. Xu et al., "Multiple window time-frequency distribution and coherence of EEG using Slepian sequences and Hermite functions," IEEE Trans. Biomed. Eng., vol. 46, no. 7, pp. 861–866, 1999.

[6] J. A. N. da Silva and M. L. R. de Campos, "Spectrally efficient UWB pulse shaping with application in orthogonal PSM," IEEE Trans.Commun., vol. 55, no. 2, pp. 313–322, 2007.

[7] C. W. Korevaar et al., "Synchronization and matched filtering in time-frequency using the unflower spiral," in Proc. IEEE Global Commun. Conf., Los Angeles, CA, USA, Dec. 2012, pp. 3959–3964.

[8] G. de Abreu et al., "Jitter-robust orthogonal Hermite pulses for UWB impulse radio- communications", EURASIP Journal Applied Signal Process., vol. 3, pp. 369 – 381, 2005.

[9] S. Savov, "An optimization of a voltage pulse excitation in a UWB radio system", IEEE Trans. Antennas & Propag., vol. 55, pp. 139 – 142, Jan. 2007.

[10] B. Farhang-Boroujeny and C. H. Yuen, "Cosine modulated and offset QAM filter bank multicarrier techniques: A continuous-time prospect," EURASIP J. Adv. Signal Process., vol. 2010, p. 6, 2010.

[11] L. E. Miller, "Autocorrelation functions for Hermite-polynomial ultrawideband pulses," IET Electron. Lett., vol. 39, no. 11, pp. 870–871, 2003.

[12] G. de Abreu, "Closed-form correlation functions of generalized Hermite wavelets", IEEE Trans. Signal Process., vol. 53, no.6, pp. 2258 v- 2261, 2005.

[13] L. Cohen, "Time frequency-distributions—A review," Proc. IEEE, vol. 77, no. 7, pp. 941–981, 1989.

[14] C.W. Korevaar et al., "Fourier-Hermite communications; where Fourier meets Hermite", IEEE Proc. ICASSP conference, pp. 4723 – 4727, 2013.

[15] C.W. Korevaar et al., "Closed-form expressions for time-frequency operations involving Hermite functions", IEEE Trans. Signal Process., vol. 64, no. 6, pp. 1383 – 1390, 2016.

[16] Gradshteyn and Ryzhik, "Tables of Integrals, Series and Products", p. 852 (in Russian).

# DIFFUSION MODELS ON TRIANGULATED SURFACES
# (selected from CEMA'21 Conference)

N. Ampilova*

* St. Petersburg State University, Comp. Sci. Dept.

Email : n.ampilova@spbu.ru

**Abstract**

*Diffusion processes occur in many scientific areas; they are especially important in chemistry, biology and medicine. Most of the mathematical models that describe diffusion are nonlinear Partial Differential Equations, which do not have analytical solutions and numerical methods require large computing resources. There is a growing interest in the structures (fractal clusters) generated by diffusion processes, and the search for new models has intensified. The important method complementary to mathematical models is imitation modeling in which the space mobility of the particles of a substance is directly modeled.*

*There are two directions in such an approach: an imitation of random walks of particles; and cellular automata modeling. In this work, for the modeling of the fractal cluster growth on triangulated surfaces, we implement algorithms based on random walk. We use classical variants of Diffusion Limited Aggregation (DLA) and Reaction Limited Aggregation (RLA) models. It is shown that, in the framework of the classical Cluster Aggregation (CCA) model, fractal cluster on a triangulated surface cannot be correctly constructed without additional assumptions about the cluster restructuring.*

*The software is written in Python; it may be used by both researchers and students as a tool for the modeling of complex processes.*

## 1. INTRODUCTION

Diffusion is one of main processes when two substances interact. Hence mathematical and imitation modeling are common tools for research. Mathematical models often do not have analytical solutions. We need therefore to apply numerical methods and imitation modeling in which a mobility of particles is simulated directly. Such an approach allows visual representation to be obtained of the objects which appear as a result of diffusion both on surfaces and in the space. Complex structures generated by various diffusion processes are called aggregates, or fractal clusters, due to their similarity with well-known objects. In reality, aggregates may be not only fractals but multifractals as well.

The active studying of such structures began in 1970 and has continued successfully up to now. Fractal aggregates appear in the process of crystallization [8] and hemagglutination [14]. Imitation modeling of the growth of fractal clusters in an environment that has given physical properties may help in forecasting results of the process under study. This technique was efficiently applied to the study of the spread of cancer cells in blood [16].

The models of the construction of fractal clusters can be divided into the following properties [13]:

- The nature of a process (cluster-particle or cluster-cluster).
- The nature of the association of particles or clusters depending on the probability of sticking.
- The nature of the motion of particles or clusters (chaotic or directional).

In 1981 W. Witten and L. Sander proposed the first computer model (DLA) [15] which constructs a fractal cluster on the plane as a result of random walks of particles which are thrown one by one. This model was then widened and modified, which resulted in: the description of RLA, which allowed the addition of a physical parameter of a given environment; and the CCA model, which considered the motion of clusters not particles.

Another approach to diffusion modeling is based on a widened notion of cellular automata. In this notion any alphabet, transition functions and regimes of the change of cell states are possible. Such a wide interpretation of cellular automata allows us to construct mathematical descriptions of space-time processes of various nature including the processes with self-organization ([1],[4]).

In practical applications, it is important to use modeling both on surfaces and in the space. The approach based on cellular automata implementation of DLA on the bone surface was proposed in [4]. In [2] the author designed and implemented the optimized DLA algorithm on a triangulated surface, which is based on the random walk method. The CCA model was applied to study processes in colloidal solutions and aerogels; the implementation was made in space configuration [10,11,17].

This work is based on random walk imitation modeling for DLA, RLA, and CCA models. Optimized DLA and RLA are realized on a triangulated surface. For CCA it is shown that, in the framework of the classical model, a correct implementation on a triangulated surface is impossible without an assumption about the cluster restructuring.

The software written in Python includes :

- Triangulation of a surface by the marching method.
- Implementation of both base and optimized DLA for a triangulated surface.
- Implementation of RLA for a triangulated surface.
- Implementation of CCA on a square lattice.
- Visualization of results in 3D.

The paper is organized in the following way. In sections 2 and 3 there is a description of the DLA model and its optimization both on the plane and a triangulated surface. The CCA model is discussed in section 4. In section 5 we describe the RLA model. The results of numerical experiments are given.

## 2. DLA MODEL

### 2.1. Witten-Sander base model

In this variant, particles are thrown on the plane randomly and walk by random way on a square lattice. The initial particle is considered as a cluster. Every next particle may move with equal probability in 4 directions – up, down, left, right – on the lattice lines or cells. A particle joins the cluster if it is a neighbor of a particle in the cluster. The choice of a way of moving depends on the representation of a particle – it may be presented by a vertex of the lattice or by a cell. The representation naturally influences the visualization results.

### 2.2. DLA on triangular lattice

In this case, we should define the directions of the particle transitions. For a particle in a triangle with sides a, b, c, define the probabilities *p(a), p(b), p(c)* to move in neighboring triangles through corresponding sides as follows:

$$p(a) = \frac{1/a}{1/a + 1/b + 1/c}$$
$$p(b) = \frac{1/b}{1/a + 1/b + 1/c} \quad (1)$$
$$p(c) = \frac{1/c}{1/a + 1/b + 1/c}$$

For example, in the triangle with sides 3, 4, 5 we have p(a)=20/47, p(b)=15/47, p(c)=12/47. The unit segment is divided as [0, 20/47, 35/47, 1]. If the random number is in the first interval, we go to the neighboring triangle through side a, etc.

## 3. OPTIMIZATION OF THE DLA ALGORITHM

In applications, the base DLA model has some disadvantages:

1. Every particle moves on a lattice chaotically and the number of steps is unbounded. Hence for large surfaces the number of steps which are required to join to a cluster grows indefinitely. Thus, for a large number of particles the run time may be unpredictably large.
2. In real experiments one usually models several clusters on the same surface. But this fact is not taken into account, which also results in the run time growth.

It follows that in real modeling we have to use some restrictions on the number of particles, size of the surface, and the number of particles in the cluster. Moreover, we consider a variant of optimization based on a reduction of the number of random walking.

### 3.1. Optimization on square lattice

The optimization proposed in [2] defines a particle's position when it joins a cluster in advance – at the moment when the particle is thrown on the lattice. For a square lattice with M cells we compute a matrix of choice of coefficients G [M, M] which is used to define the particle position.

When a particle is thrown on a lattice the choice coefficients are calculated for each boundary point of the cluster. It is known [2] that these coefficients depend on only the sum of coordinate distances (a on abscissa and b on ordinate) between a new particle and boundary points of the cluster and may be calculated as:

$$p(a,b) = \frac{1}{4(a+b)} \tag{2}$$

We consider the obtained coefficients as values of a distribution function, choose a value randomly, and the preimage of this value defines the position of joining.

### 3.2. Optimization on a surface

For a triangulated surface we present the structure of a lattice by a graph, such that triangles correspond to the graph vertices, and edges between vertices mean that these triangles are adjacent. Define on edges (paths by length 1) weights (choice coefficients) which are calculated by (1). Write these weights in a matrix $G_1$. Then construct a sequence of matrices $\{G_k\}$, such that $G_k$ contains choice coefficients for k-length paths. The weight of a path equals the product of weights of edges.

In $G_1$ denote by $p(i,j)$ the weight of the edge (i,j). Let $p(i,j) = y$, and $p(j,j_1) = y_1$, $p(j,j_2) = y_2$, $p(j,j_3) = y_3$ for neighbors of $j$. Then in $G_2$ in elements with indices (i,$j_1$), (i, $j_2$), (i, $j_3$) the coefficients $p(i,j_1) = yy_1$, $p(i,j_2) = yy_2$, $p(i,j_3) = yy_3$ will be written. Thus $(i,j_1)$ corresponds to the 2-length path from i to $j_1$ and its weight is the product of the weights of the path edges. The matrices of higher order are constructed by analogy.

The common matrix of the choice coefficients is calculated as the sum of $G_k$, where k is from 1 to a given N. The position of the place of joining the cluster is defined by the analogy with the case 3.1. The optimized algorithm may require more or equal time than the base one. The optimization results in considerable time gain when we conduct a series of experiments, because the matrix G is calculated one time for a given surface.

Summing up one may say that:

1. When modeling one cluster, the base and optimized algorithms show close results. The optimized variant may be slower if the number of triangles is large.
2. When modeling the large number of clusters, the optimized algorithm reduces run-time considerably.

The optimized algorithm for a triangulated surface was implemented in [3]. In the next table the results of both algorithms on the surface $\boldsymbol{x^3 + y^2 + z = 0}$ are given. The number of triangles is 4000, the number of particles in the cluster is 500.

Table 1. The comparison of base and optimized DLA algorithms

| The number of clusters | Base DLA | Optimized DLA |
|---|---|---|
| 1 | 5m 56s | 6m 59s |
| 5 | 53m 11s | 11m 41s |

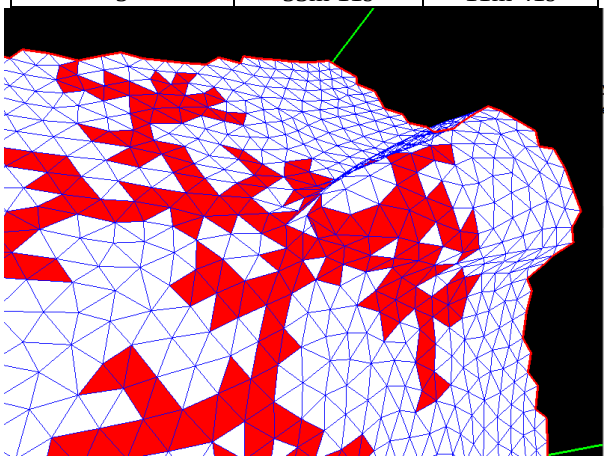

Figure 1. The result obtained by optimized DLA on the surface $\boldsymbol{x^3 + y^2 + z = 0}$

## 4. CCA MODEL

### 4.1. CCA on square lattice

This model was proposed in [9]. Compared with a particle-cluster model, in this model the common number of particles is known and all of them are on a surface (or plane).

The particles randomly walk on the lattice. When 2 particles collide they join into a cluster, and this cluster continues to walk. It is assumed that the probability of collision of 3 or more clusters is very small. At the end of the modeling, we have a final aggregate.

The movement of a cluster on a square lattice is similar to the movement of a particle – on every step the cluster may move one cell left or right or up or down with equal probability. Clusters are considered to be sticky if at least one particle of the first cluster is on the cell which is the neighbor of a particle of the second one. In such a situation, due to the structure of square lattice, a cluster moves as a single whole and saves its structure.

### 4.2. Problems of CCA on triangular lattice

On a triangular lattice we cannot always model the cluster movement to save its structure. To explain the situation, we give the following definitions. We call the movement of a cluster ***correct*** if :

(1) Every particle of the cluster passes through the same number of the cells of the lattice.

(2) The number of particles does not change, i.e. the structure is preserved.

The movement of a cluster is ***semi-correct*** if only (1) or (2) holds. The movement is ***incorrect*** if it is not correct or semi-correct.

It is easy to note when the movement of a cluster on square grid is correct, because all the particles pass the same distance in a chosen direction and the structure is preserved.

On a regular triangular grid, the movement of a cluster may be only semi-correct. In this case different particles may pass different distances and move in different directions. Hence, to save the structure, the cluster must turn. In other words, we cannot move the cluster as a single whole. Such a situation is explained by the structure of triangular lattice.

In Figure 2 the red cluster in the left part of the picture moves on 1 cell in the direction marked by the black arrow. On the right side its initial position (blue color) and the result of the movement (red color) are shown. We see that some particles pass 1 cell, and one particle should pass 3. The cluster makes 1 step, but to make it possible the particles should pass a different number of cells. According to our definition, the

movement is semi-correct because condition 1) does not hold. Note that this situation is possible only or regular triangular lattice on the plane.

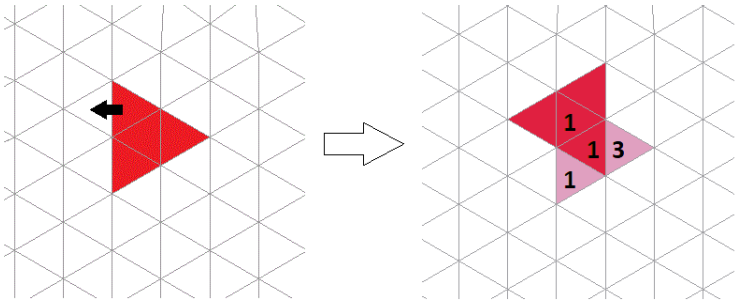


Figure 2. The example of the motion of a cluster on a regular triangular grid: particles of the cluster make a different number of steps

For non-regular triangular lattice, the nodes of the lattice may have a different number of neighbors; it does not allow the structure of a cluster to be preserved. This situation is illustrated in Figure 3. The blue cluster consists of 5 particles; every particle has 2 neighbors. We cannot move it into the red area without changing the structure.

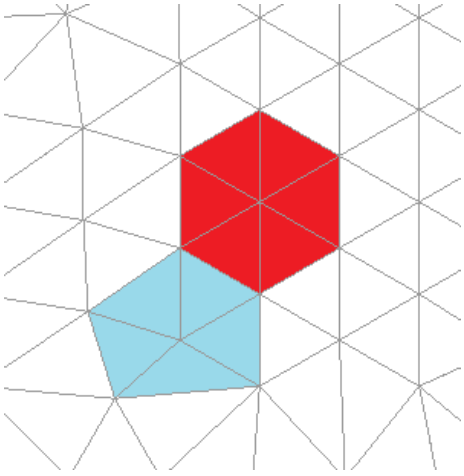

Figure 3. Restructuring on non-regular grid: blue cluster cannot be moved to the red area without changing its structure

Thus, it is impossible to implement the CCA algorithm on a non-regular lattice without modifications that allow the cluster restructuring. For example, in [17] the authors assumed that a cluster may spin; when 2 clusters stick together, they can spin in

the point of contact. They also proposed that there is a tension between particles, hence particles may influence each other in the process of the cluster growth. It may lead to a change of the cluster structure.

In real tasks the modeling of CCA on a surface has a limited scope of application, and the modeling in the space is more important. In this case some problems appearing for non-regular lattice on a surface may be solved and a cluster may be admitted to turn or change a structure. Such a model may be used when studying colloid solution or aerogels. In [16] an interesting variant of CCA space model in a boundary area was implemented: when a cluster collides with boundaries it moves in the opposite direction. This model may be applied to the modeling of nanoscale medicinal products [10], catalytic reactions [11] and physical properties of materials.

## 5. RLA MODEL

To take into account physical properties of a real environment, we should introduce some parameters. In this model the probability of joining a particle to a cluster is considered.

Proposed in [7] RLA (Reaction Limited Aggregation) model describes the growth of a fractal cluster when the probability of sticking is small. In [12] the authors merged CCA and RLA models, introduced the binding energy between particles, and assumed that the probability of sticking depends on the time of random walking and the time of breaking binds. Thus, the probability of sticking is a dynamical parameter.

We implemented RLA on a triangulated surface and used the probability of sticking as a parameter. This is a modification of DLA and may be performed both for base and optimized variants.

If a particle is near a cluster and the probability of sticking $p_s$ is small, it continues to walk. Denote the number of walks by $N$ and the number of walks which lead a particle to a cluster by $N_w$. Choose $N, N_w$ such that $\frac{N_w}{N} = p_s$. If after $N$ walking $N_w = 0$ (the particle did not get closer to the cluster) we delete the particle and throw a new one.

The example of the construction of the aggregate on the surface $x^3 + y^2 + z = 0$ for $p_s = 0.1$ (left) and $p_s = 1$ (right) is shown in Figure 4. The number of triangles is 1419, the number of particles is 200.

The run-time for $p_s = 0.1$ is 1m 3s, and 19s for $p_s = 1$.

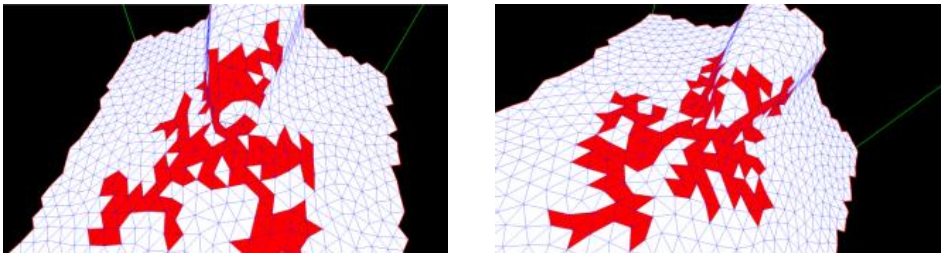

Figure 4. RLA model on the surface $x^3 + y^2 + z = 0$
$p_s = 0.1$(left) $p_s = 1$(right)

The triangulation was performed by the marching method proposed by E. Hartmann [5]. It is quite simple to implement and may be applied to any type of a surface. The size of the lattice is given by a parameter.

## 6. CONCLUSION

Mathematical models of diffusion are rather complex and as a rule do not have analytical solutions. For a successful study of diffusion processes, one should combine mathematical and numerical methods and imitation modeling. In this work, we present a program system for the imitation modeling of the growth of fractal clusters on a triangulated surface by DLA and RLA models. It is shown that CCA model cannot be implemented on a triangular lattice without a restructuring of a cluster. The program may be useful both for researchers and students.

## ACKNOWLEDGEMENTS

The author thanks G. Doronin for help in computer experiments.

**REFERENCES**

[1] O. L. Bandman. "Cellular Automata composition techniques for spatial dynamics simulation". Bulletin of the Novosibirsk Computing Center. 2008. No.27. p. 1–40.

[2] A. Batyukov. "Design and implementation of classification algorithms of digital images of biomedical preparations", Ph.D. thesis /A.M. Batyukov; St. Petersburg State University, 2015. (in Russian)

[3] G. A. Doronin "Modeli agregacii ogranichennoi diffusiei na tranguliruemih poverhnostiah".Proc. Conf. LXXIV Herzen Readings, 5-10 April, 2021, St.Petersburg, p. 218-223. (in Russian)

[4] A. Evseev. "Kletochno-avtomatnoe modelirovanie diffusionnih processov na trianguliacionnih setkah". Prikladnaia discretnaia matematika 27. Tomsk, isd. Tomskogo universiteta, 2009. No 4(6). p. 72-83.

[5] E. Hartmann. "Geometry and Algorithms for computer aided design". Department of Mathematics Darmstadt University of Technology, 2003. Geometry and Algorithms for COMPUTER AIDED ehartmann/ and Algorithms for COMPUTER AIDED DESIGN Erich Hartmann Department of Mathematics Darmstadt University of Technology October 2003 (pdfslide.net)

[6] A. Hasmy, J. Primera, T. Woignier. "Cluster–cluster aggregation with mobile impurities", Journal of Sol-Gel Science and Technology., 2019. DOI:10.1007/s10971-019-04918-3

[7] R. Julien, M. Kolb "Hierarchical model for chemically limited cluster-cluster aggregation", J. Phys.,1984, Ser. A.,V.17, P.L639.

[8] K. Kassner "Pattern Formation in Diffusion-Limited Crystal Growth". – Singapure: World Scientific, 1996.

[9] M. Kolb, R. Botet, R. Julien. " Scaling of kinetically growing clusters", Phys. Rev. Lett.,1983, V.51, P.1123.

[10] I. V. Lebedev, I. I. Khudeev, A. V. Kolnoochenko, A. Y. Tyrtyshnikov, S. I. Ivanov, N. V. Menshutina. "Silica-resorcinol-formaldehyde aerogels nanostructure modelling", Chemical Engineering Transactions, 70, 1765-1770., 2018.

[11] N. Menshutina, E. Lebedev, A. Kolnoochenko, P. Tsygankov, I. Lebedev. "Complex Modeling and Design of Catalytic Reactors Using Multiscale Approach", Part 1: Diffusion in Porous Catalyst. Computation, 8(1),11., 2020.

[12] W. Y. Shih, I. A. Aksay, R. Kikuchi. " Reversible-growth model: Cluster-cluster aggregation with finite binding energies", Phys. Rev.,1987, Ser. A. V.36, P.5015.

[13] B. M Smirnov. "Physica fractalnih clasterov", M., Nauka, 1991. (in Russian)

[14] F. Wiegel, A.Perelson. "Statistical mechanics of Red Blood cell aggregation: the distribution of rouleaux in thermal equilibrium", J.Stat.Phys. v.29, 1982.Wiegel F.,

[15] T. A. Witten, L. M. Sander. "Diffusion-Limited Aggregation, a Kinetic Critical Phenomenon", Phys. Rev. Lett., 1981.

[16] I. Zhukova, E. Kolpak. "Mathematical models of malignant tumor". Vestnik SPbGU—2014, ser. 10, n.3, c. 5-17. (in Russian)

[17] R. Zirianov. "Razvitie fractalnih modelei agregacii kolloidnih chastits". Molodoi uchenii. No. 24 (128), p. 72-76., 2016. (in Russian)

# AN ANALYSIS OF UNCERTAINTY AND STATISTICS OF HIGH DYNAMIC RANGE ACOUSTIC SIGNALS (selected from CEMA'21 Conference)

I. Simeonov*,

* Vasil Levski National Military University, Veliko Tarnovo,
76, Bulgaria Blvd., 5000, Veliko Tarnovo, Bulgaria
Email: ivanov_ivan@nvu.bg

**Abstract**

*In this paper, a number of large dynamic range acoustic signals statistics has been presented based on continuous wavelet transform. Some typical examples from battlefield acoustics and from musical acoustics are considered. Therefore, a specialized platform and a measuring microphone with the required features are used in field experiments. The characteristic acoustic environment signature and background noise features for some concrete setup are described.*

*Possible directions for using these technics for signal statistics analysis for retrieving useful information, based on Shannon entropy, are outlined. The datasets consisting of the raw data and metadata from bell ringing and gunfire, and noise recordings are estimated. The wavelet transform was of particular importance here, as it provides both constant-bandwidth analysis that correlates with sound perception and optimal resolution. The discussed problems by means of continuous wavelet transform (CWT) and decomposition (or Shannon) entropy are approached. The results can be used in various areas of acoustics and electrodynamics.*

## 1. INTRODUCTION

In the recent years, some application of modern acoustic methods in interdisciplinary fields and discovery of the difficulties when signal processing and storing of high dynamic range acoustic data, such as music, noise of natural phenomena, battlefield acoustic, and others was regarded [1, 2, 3].

Many acoustic data from field experiments have been collected since 2008 at different sites. Wavelet analysis offers a way to process this acoustic data collection and it provides possibility to made interesting considerations about their characteristics.

The analysis based on Shannon entropy have been powerful and useful in determining the noise influence.

The aim is presenting one direction for using technics for signal statistics analysis for retrieving useful information, based on Shannon entropy and wavelet processing.

## 2. SHANNON ENTROPY PROPERTIES IN ACOUSTIC DATA PROCESSING

In Donoho et all work, [4] is discussed some of the lessons of harmonic analysis in the XX century and the authors made this interesting possible connection between the compression, and not only compression, of real data, concerns random, and the deterministic objects analysis following Tikhomirov's words:

"our vast mathematical world" is itself divided into two parts, as into two kingdoms. Deterministic phenomena are investigated in one part, and random phenomena in the other.

To Kolmogorov fell the lot of being a trailblazer in both kingdoms, a discoverer in their many unexplored regions he put forth a grandiose programme for a simultaneous and parallel study of the complexity of deterministic phenomena and the uncertainty of random phenomena, and the experience of practically all his creative biography was concentrated in this programme.

From the beginning of this programme, the illusory nature of setting limits between the world of order and the world of chance revealed itself" [4,5].

The ideas of entropy of the signal or signal uncertainty and its measure (bits per signal units) was defined in communication theory.

In Stratonovich work [6], Shannon entropy for a continuous random variable with p.d.f. $p(\xi)$ is defined as an expectation :

$$H_\xi = \mathrm{E}[p(\xi)] = -\int_{\mathbf{X}} p(\xi) \ln p(\xi)\, d\xi \tag{1}$$

or

$$H_\xi = -\int_{\mathbf{X-\Lambda-\Lambda_0}} \ln \frac{dP}{d\nu}(\xi) P(d\xi) \tag{2}$$

in case $\nu_0(\xi) = dv/d\xi = 1$.

In other side Shannon entropy can be defined with Kullback–Leibler divergence:

$$\mathrm{H}(\boldsymbol{X}) = \mathrm{E}[\mathrm{I}_{\boldsymbol{X}}(x)] = \log(N) - D_{KL}\big(p_{\boldsymbol{X}}(x) \parallel P_U(\boldsymbol{X})\big) \tag{3}$$

Then, H($\boldsymbol{X}$) is the number of bits which would have to be transmitted to identify $\boldsymbol{X}$ from $N$ equally likely possibilities, less the relative entropy of the uniform distribution on the random variates of $\boldsymbol{X}$, $P_U(\boldsymbol{X})$ from the true distribution P($\boldsymbol{X}$).

The *relative entropy* or *Kullback–Leibler distance* between two probability mass functions *p(x)* and *q(x)* is defined, [7] as

$$D_{KL}(p \parallel q) = \sum_{x \in \mathcal{X}} p \log \frac{p}{q} =$$

$$= E_P \log \frac{p(X)}{q(X)} \tag{4}$$

Some useful properties of Kullback–Leibler divergence was demonstrated also in R. Angelova-Slavova's works [8, 9].

The known analogy with quantum systems, is in Sanchis-Alepuz paper [10] where the Shannon's information entropy defined by :

$$Su = -\int \mathcal{P}(\mathrm{r}) \ln \mathcal{P}(\mathrm{r}) d\mathrm{r} \tag{5}$$

Probability distribution function $\mathcal{P}(\mathrm{r})$ similarly to electronic density distribution here is normalizing the square of the displacement field of a given acoustic level

$$\mathcal{P}(\mathrm{r}) = |u(\mathrm{r})|^2 / \int |u(\mathrm{r})|^2 d\mathrm{r} \tag{6}$$

and this quantity gives the uncertainty of the localization of sound in acoustics problems.

## 3. WAVELET ANALYSIS AND SHANNON ENTROPY

The wavelet transform is used to decompose a mixture of signals and noise, into components at different resolutions and make some conclusions about noise features. It is

known that the finer scales in the continuous wavelet transform (CWT) gives a higher-fidelity signal analysis. It can be better describe oscillations or localize signal transients, with the CWT than with the discrete wavelet transforms.

One regard to wavelets, which can be viewed as an information processing technique can be found in Oliveira's work, [11] where the concept of wavelet mutual information between a signal and an analyzing wavelet is introduced.

The Shannon entropy of some orthogonal wavelets, like Daubechies, Symmlets, Coiflets, that cannot be described by analytical expressions can be found by using the so-called two-scale relationship of a multiresolution analysis. In [11] a few simple discrete signals were analyzed in order to gain insight into the information theory approach for multiresolution analysis.

One possible method for measurement of entropy of discrete signal wavelet packets, [12,13] is expressed as:

$$\mathrm{WPE_N} = -\sum p_{j,n} \log p_{j,n} \tag{7}$$

where $\mathrm{p_{j,n}} = \mathrm{E_{j,n}}/\mathrm{E_{tot}}$ - relative energy for scale j,

$$\mathrm{E_{j,n}} = \sum_k \left|\mathrm{d_{j,n}}(k)\right|^2, \ \mathrm{E_{tot}} = \sum_n \mathrm{E_{j,n}} \tag{8}$$

$$\mathrm{p_{j,n}} = \frac{\sum_k \left| 2^{\frac{j}{2}} \int_{-\infty}^{\infty} \mathrm{s(t)}\, \psi_n(2^{-j}\mathrm{t} - \mathrm{k})\mathrm{dt} \right|^2}{\sum_n \mathrm{E_{j,n}}} \tag{9}$$

$\mathrm{s(t)}$ is original signal,

j, n, k represents the scale, band, and surge parameter, respectively.

Equation for $\mathrm{WPE_N}$ uses the Shannon method to calculate WPE. The N notation in $\mathrm{WPE_N}$ is used to denote the level of decomposition used in Wavelet packet decomposition.

The idea is that the accuracy of the selected wavelet basis is higher when the entropy is small.

## 4. WAVELET ANALYSIS AND SHANNON ENTROPY OF EXPERIMENTAL ACOUSTIC DATA

The interaction of the acoustic wave with objects, such as the ground, obstacles, the effects of reverberations, first reflections, absorption, interference and diffraction, turbulence etc. will change the registered sound pictures in real setups, [14,17].

The sound picture and noise level is varying in accordance of type of concrete space: close or free space, in dependence of source and receiver points placement. They change depending on the local parameters as temperature, wind speed and direction, air pressure and humidity etc.

In the next it was made the analysis of a set of experimental data and it was found the wavelet entropies of the different sound records.

First it was regarded the unique bell sounds in close space. The signals, see project Bell [1,3] denoted as Melnik2-1220 AD, was registered inside the hall in National Historical Museum in Sofia. In the figures 1a) and b) was shown some bell strike

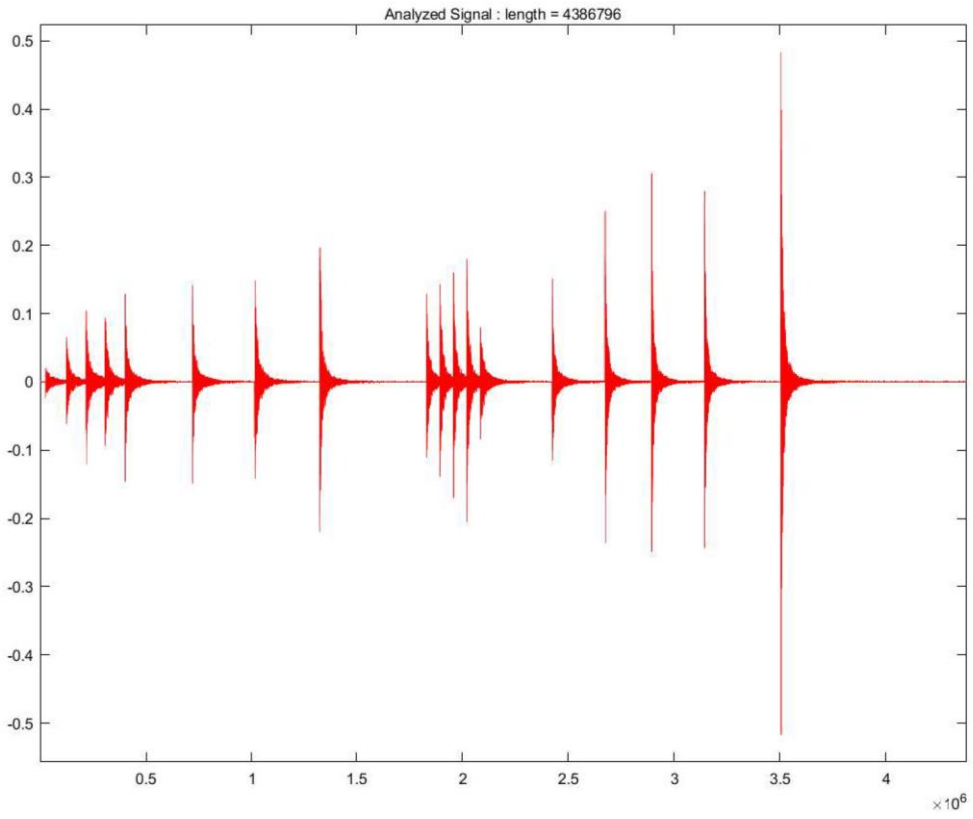

waveforms (ringing) in time.

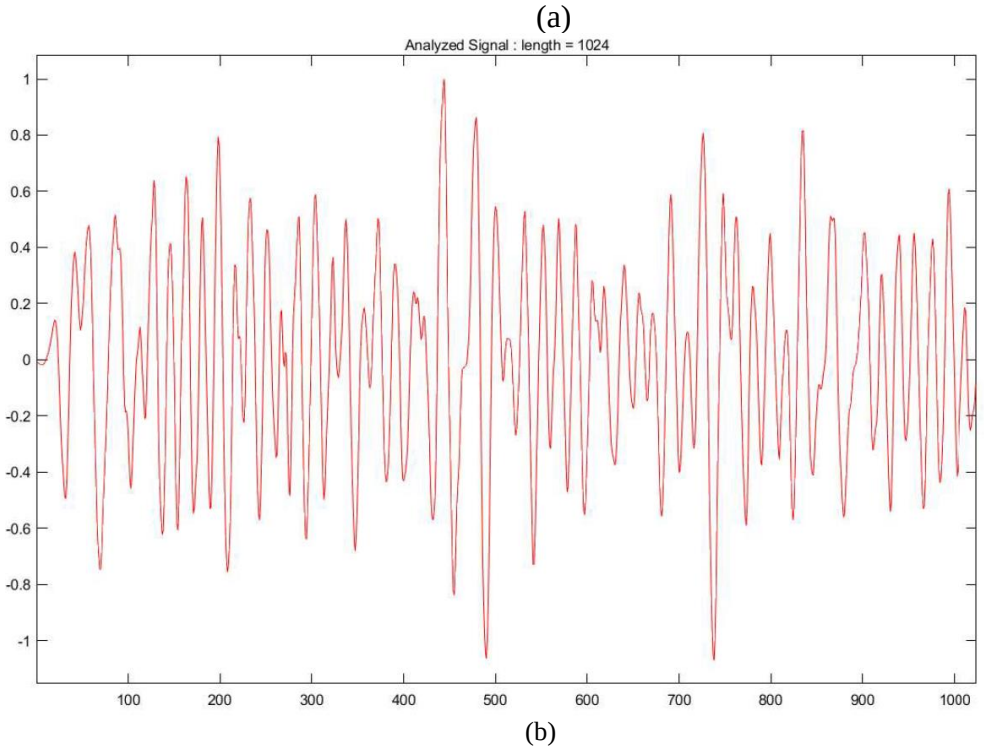


Figure 1. Waveforms of unique bell stroke (XIII cent.), (a) ringing, (b) it was separated only last bell ring.

Zoomed fragment of last bell strike in the time scale are shown in Fig.1b).

Second signal, illustrated on a Fig.2 consist a parts from time signal from the first blast from 122 mm 2S1 howitzer ("Gvozdika ") see [15], where in a) is shown the signal captured from two blasts from the two howitzers ("Salvo"), in b) the first from two blasts, 1024 samples.

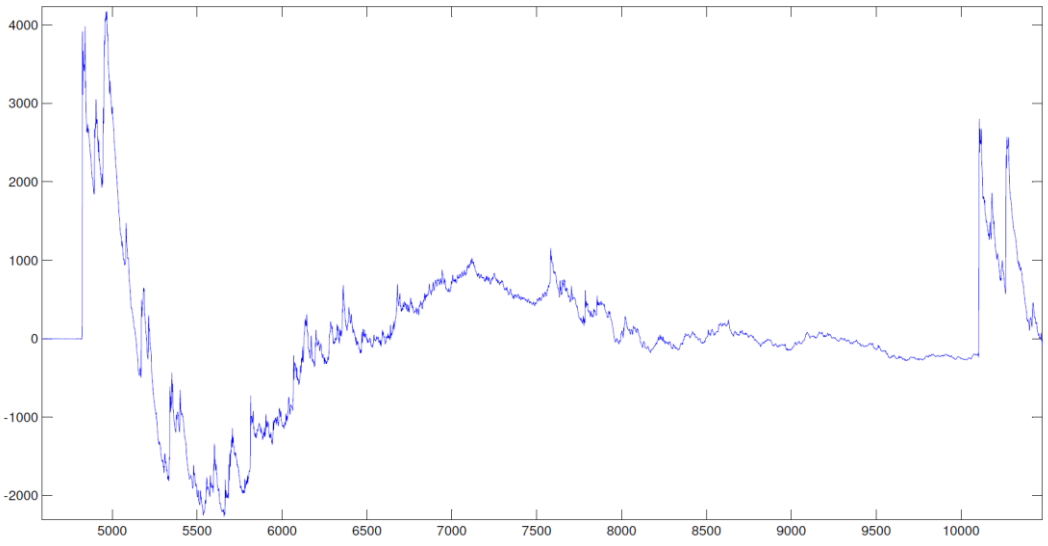


(a)

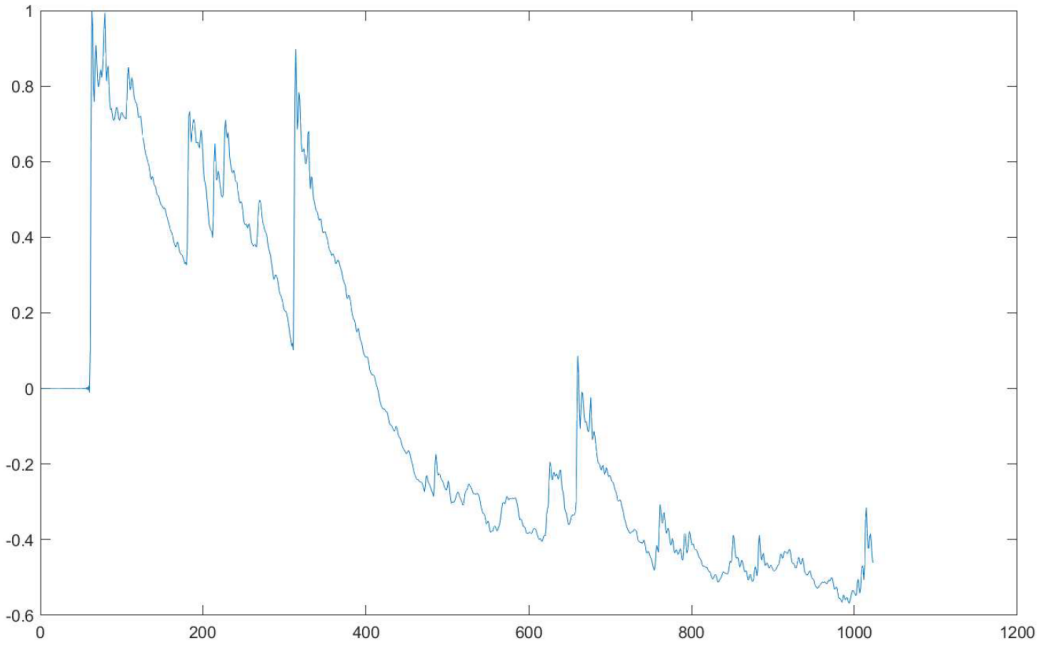


(b)

Figure 2. Parts from time signal from the first blast from 122 mm 2S1 howitzer, (a) “Salvo”, (b), the first from two blasts.

And in third, record of noise of hailstone strikes, plus noise of auto alarms was regarded, see Fig. (3a), and zoomed part in Fig. (3b). The hail dropping strikes conditions, 20 May 2013, in concrete urban environments can be seen in [16].

This raw data was exported in MatLab and here were determined Shannon entropy coefficients for the wavelet tree for Daubechies3 wavelet level 3. Fig. 4 shows wavelet packets for three parts of bel ringing waveform (Fig. 1).

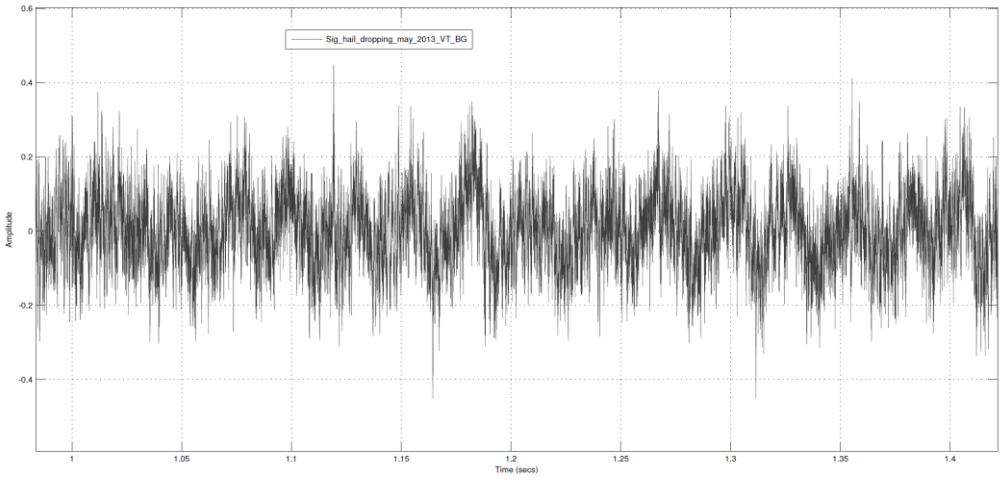


(a)

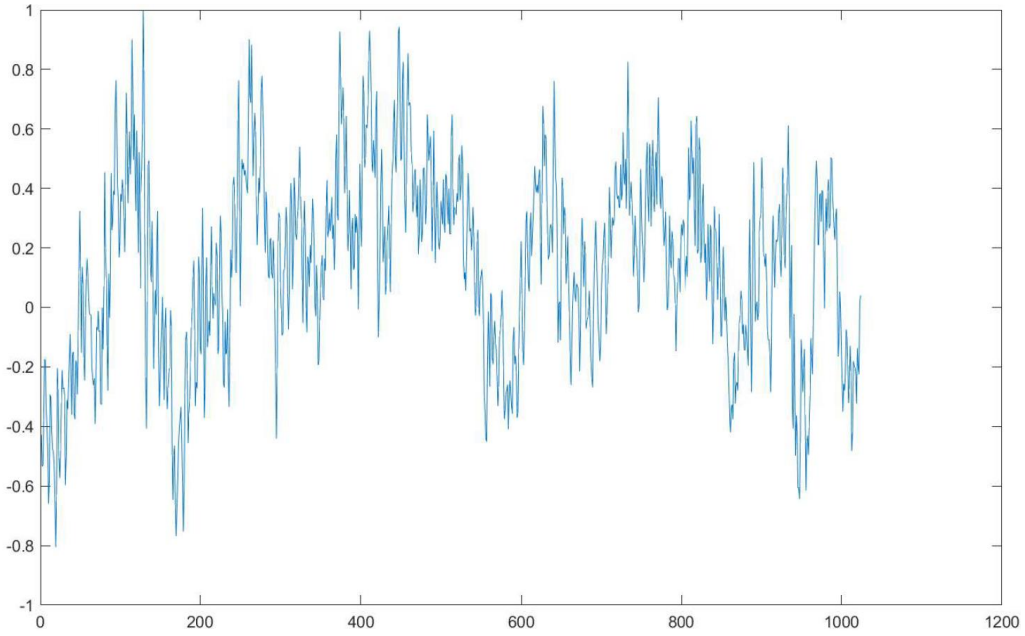

(b)

Figure 3. (a) Part of waveform of hail strikes, 0.4sec, in V. Tarnovo, BG, urban environments, 20 May 2013, (b) 1024 samples of hail strikes - zoom part of (a), Fs=65536Hz.

The wavelet packet entropies for concrete bel ringing signals in hall, totally 3 examples (noise, noise and part of ring, ring) were calculated and some results are shown

in table 1. In table is shown entropies for the simulated noise with normal and uniform distribution.

Analogically wavelet packet entropies for the signals from blast Fig.2 and hail strikes Fig. 3 were calculated. Part of results is shown in Table 2.

From wavelet packet entropies presented in table 1,2 can be seen that for noise and for signal with noise the coefficients of Shannon entropy ShE(1,1) has higher values, than other situations.

Then the proportion of ShE(1,0) and ShE(1,1), and ShE(j,0) and ShE(j,1) i.e. entropy of approximation coefficients to detail coefficients may be parameter for noise discrimination.

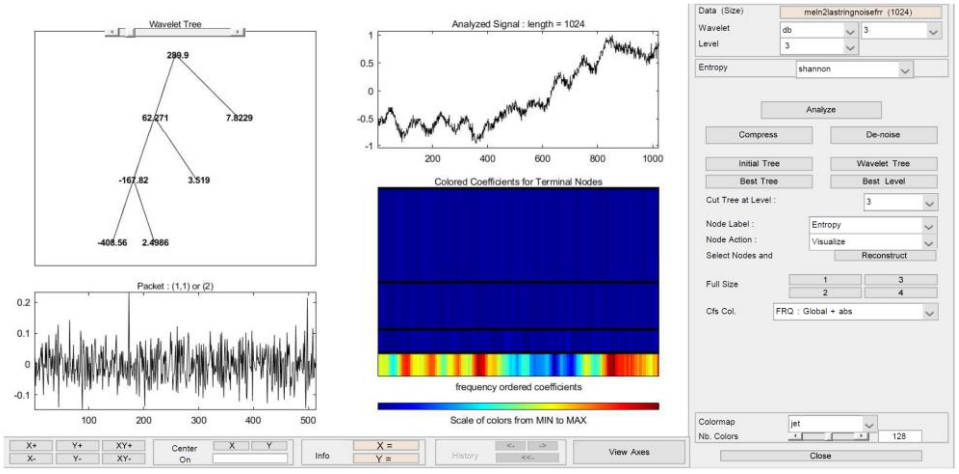


(a)

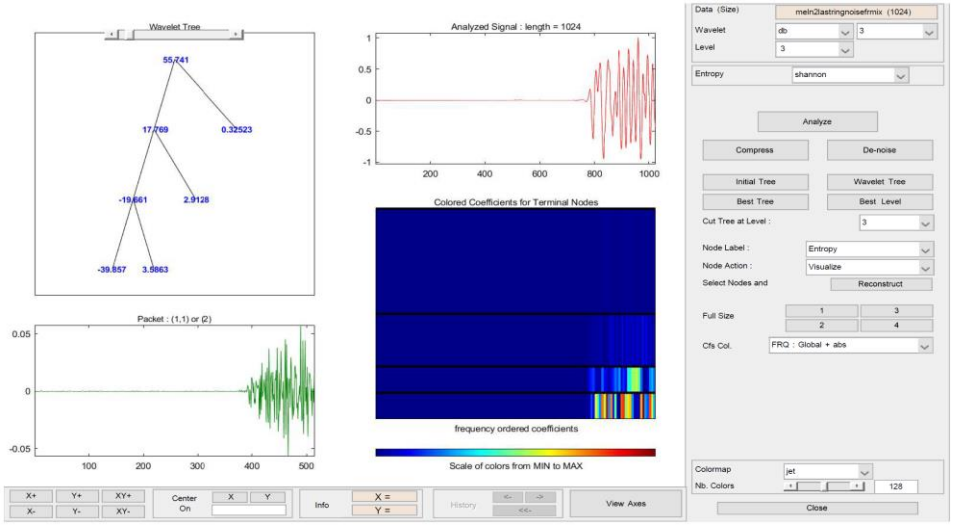


(b)

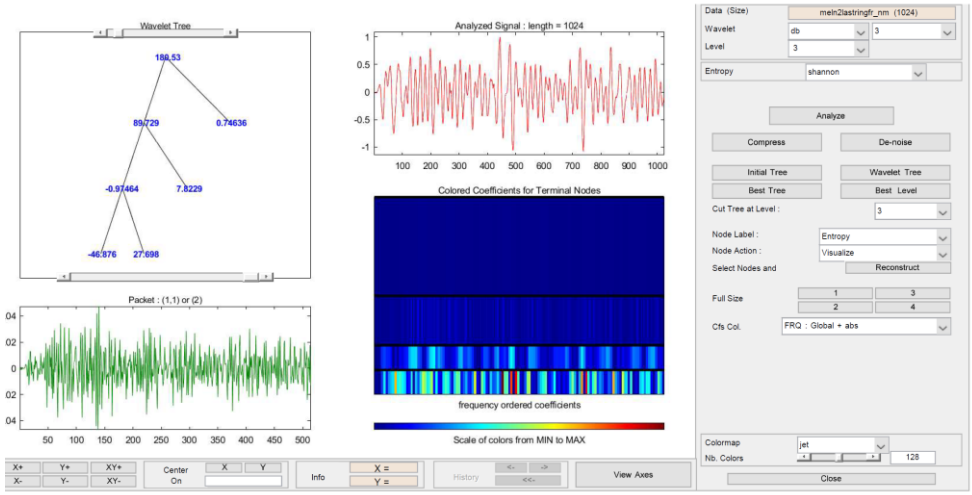


(c)

Figure 4 Calculated wavelet packets and Shannon entropies for three cases: (a) noise, (b) noise and ring, and (c) ring, see. Fig. 1 the last ring, (Daubechies db3, level 3).

Table 1.

| s name (1024 samples) | ShE(0,0) | ShE(1,0) | ShE(1,1) |
|---|---|---|---|
| Noise | 289.9 | 62.271 | 7.823 |
| Ring_Noise | 55.741 | 17.769 | 0.32523 |
| Ring | 180.53 | 89.729 | 0.74636 |
| | | | |
| Uniform distr. simulation | 220.2 | 79.51 | 79.273 |
| Norm distr. simulation | 141.85 | 71.464 | 68.755 |

Table 2.

| s name (1024 samples) | ShE(0,0) | ShE(1,0) | | ShE(1,1) |
|---|---|---|---|---|
| Front of blast artil. | 248.93 | 119.26 | | 0.77904 |
| Hail2013 | 186.35 | 105.22 | | 19.441 |
| | | | | |
| Uniform distr. simulation | 220.2 | 79.51 | | 79.273 |
| Norm distr. simulation | 141.85 | 71.464 | | 68.755 |

In audio fingerprinting the background noise is one of degradation factors like as pitching, equalization, analog to digital conversion, audio coders etc. When the purpose is automatically recognizing the type of sound recording Papaodysseus [18] and Roussopoulos [19], proposed recognition system of musical recordings in the presence of noise. The main idea in this works is the assumption of existing of invariant characteristics in time – frequency domain, which are independent of distortion and the system employs a set of mathematical characteristics, extracted from a musical recording, whose determination was based on human perception. In the other side if the purpose is automatically recognizing the type of location from which the signal is received it can be applied data mining methods like it was presented in [20].

## 5. CONCLUSION AND FUTURE RESEARCH

As it shown proportion of entropy of approximation coefficients to detail coefficients in entropy of discrete signal wavelet packets may be one parameter for noise discrimination.

The obtained results show acceptable accuracy in many real acoustic situations. It was demonstrated that wavelet processing and Shannon entropy was appropriate to analysis the characteristics of acoustic signals.

The future work will be related to their application in aerial acoustics, in interdisciplinary fields such as, study of noise from natural phenomena, ecology, battlefield acoustics and others.

## ACKNOWLEDGEMENTS

I would also like to thank Prof. Tihomir Trifonov from Vasil Levski National Military University for his advice and for creating an exceptional atmosphere of inspiring interest in acoustic signal processing.

I would also like to extend my thanks to Dr. Georgi Dimkov from the Institute of Mathematics and Informatics, Bulgarian Academy of Sciences, for his collaboration in projects and for providing the hardware 'PULSE'.

## REFERENCES

[1] The Bell Project - Research and Identification of Valuable Bells of the Historic and Culture Heritage of Bulgaria and., 2008 [Online] Available: http://www.math.bas.bg/bells/belleng.html

[2] V. Fol, G. György, T. Trifonov, A. Alexiev, I.S. Ivanov, "Acoustic Characteristics of Sacral Thracian Sites," in Proc. 11th Int. Symp. on Applied Informatics and Related Areas (AIS 2016), Székesfehérvár, Hungary, Nov. 17, 2016, pp. 84-87.

[3] T. Trifonov, I. Simeonov, N. K. Yordanov, "Advanced Signal Processing Methods For Analysis Of High Dynamic Range Acoustic Phenomena," in Proc. 13th Conf. on Communications, Electromagnetics and Medical Applications (CEMA'18), Sofia, Bulgaria, Oct. 18-20, 2018, pp. 52-56, ISSN: 1109-1606.

[4] D.L. Donoho, M. Vetterli, R. A. DeVore, and I. Daubechies, "Data compression and harmonic analysis," IEEE Trans. on Inform. Theory, vol.44, no.6, pp. 2435-2476, 1998.

[5] V. M. Tikhomirov, “Widths and entropy,” Usp. Mat. Nauk, vol. 38, pp. 91–99, 1983 (in Russian), English transl. in Russian Math Surveys, vol. 38, pp. 101–111.

[6] R. L. Stratonovich “Teoriya informacii,” (in Russian) (“Information Theory”). Moscow, Sov. radio, 1975, ch.1, sec.6, pp. 31-34.

[7] Thomas M. Cover and Joy A. Thomas, “Elements of Information Theory.” John Wiley & Sons, 2nd edition, 2006.

[8] R. L. Angelova-Slavova, “Convergence and applications of the Metropolis - Hastings Algorithm,” Plovdiv, Bulgaria, Astarta, 2020. ISBN 978-954-350-284-4 (in Bulgarian).

[9] R. L. Angelova-Slavova, “Some Properties of the Kullback – Leibler Divergence,” Annual of NVU "V. Levski" 2020, part 2, V. Tarnovo, pp.62-68, 2021. ISSN 1312-6148 (in Bulgarian).

[10] H. Sanchis-Alepuz and J. Sánchez-Dehesa, “Shannon Entropy as a Characterization Tool in Acoustics,” J. of the Acoustical Society of America, vol.123, no.5, pp. 3280 -3280, 2008.

[11] H. M. de Oliveira and D. F. de Souza, "Wavelet analysis as an information processing technique," 2006 International Telecommunications Symposium, pp. 7-12, 2006, doi: 10.1109/ITS.2006.4433232.

[12] A. Rizal, R. Hidayat, H.A Nugroho, “Comparison of multilevel wavelet packet entropy using various entropy measurement for lung sound classification,” Int. Journal of Advanced Computer Science and Applications, vol.210, no.2, pp.77-82, 2019.

[13] O. A. Rosso, S. Blanco, J. Yordanova, V. Kolev, A. Figliola, M. Schürmann and E. Başar, “Wavelet entropy: a new tool for analysis of short duration brain electrical signals,” Journal of neuroscience methods, vol. 105, no.1, pp.65-75, 2001.

[14] Tihomir Trifonov, Fundamentals of sound engineering: [Textbook for VVOVU V. Levski - V. Tarnovo] - Sofia: Ministry of Defence St. George the Victorious, 1995. (in Bulgarian).

[15] N. Yordanov, T. Trifonov, I. Simeonov, “An experimental investigation of the 122mm artillery system firing acoustic field,” Int. sci. J. Security&Future, Year I,

Iss. 4, Sofia, Dec. 2017, Sofia, Bulgaria, Scientific technical union of mechanical engineering Industry-4.0, pp. 160-162, ISSN: 2535-082X.

[16] I. S. Ivanov, É. Hajnal, "Characteristics of Hail Dropping Noise in Urban Environment," J. "Mathematics, Computer Science and Education" vol. 1, no. 1, pp. 37–43, 2018, "St. Cyril and St. Methodius" University of V. Tarnovo, Bulgaria, ISSN: 2603-4670 (Print).

[17] T. Trifonov, Statistika, V. Tarnovo, Bulgaria, Faber, 2012, ISBN 978-954-9498-18-9 (in Bulgarian).

[18] C. Papaodysseus, G. Roussopoulos, D. Fragoulis, T. Panagopoulos and C. Alexiou, "A new approach to the automatic recognition of musical recordings," J. Audio Eng. Soc., vol. 49, no. 1/2, pp. 23–35, 2001.

[19] G. Roussopoulos, D. Fragoulis, C. Papaodysseus, Ath. Panagopoulos and M. Exarhos, "Mathematical Characteristics for the Automated Recognition of Musical Recordings," WSEAS Transactions on Mathematics, Issue 3, vol.3, pp. 698-704, July 2004, ISSN: 1109-2769.

[20] I. Simeonov, T.Trifonov, T. Georgieva-Trifonova, "Signal Processing and Storing of High Dynamic Range Acoustic Data for Knowledge Discovery," in Proc. of 14th Int. Conf. Communications, Electromagnetics and Medical Applications (CEMA'19), Sofia, Bulgaria, October 17th-19th, 2019, pp. 58-62, ISSN: 1314-2100.

# REVISITING ENHANCED AIS DETECTION RANGE UNDER DUCTING

## (selected from CEMA'21 Conference)

I. Sirkova*

* Laser Radars Lab, Institute of electronics, Bulgarian Academy of Sciences

Tzarigradsko chaussee 72, 1784 Sofia, Bulgaria

Email: irina@ie.bas.bg

**Abstract**

*This report studies the propagation of Automatic Identification System frequencies under various tropopheric ducting and sea surface conditions with the parabolic wave equation method. The aim is to examine the influence of sea surface roughness on the possibility to enlarge the AIS detection range under ducting.*

## 1. INTRODUCTION

Initially designed as a ship reporting system for collision avoidance, the AIS (Automatic Identification System) nowadays has enlarged applications beyond the situational awareness and security. The AIS has become part of the VHF Data Exchange System concept [1] which increases the requirements to the AIS performance and reliability. At the same time, the growing importance of the AIS traffic poses the need to monitor shipping at distances greater than can be achieved via the conventional propagation mechanisms like line-of-sight (LoS) and diffraction. Thus the long range detection capability becomes a key AIS characteristic. Among the factors that can influence the long range detection of AIS messages the ducting anomalous propagation mechanism, often present over the sea, is identified as a major candidate [2]. This clear-air propagation mechanism is due to deviation in tropospheric refractivity $N$ ($N=(n-1)10^6$) from the standard conditions caused by temperature and water vapour changes. The spatial change of $n$ is larger with height than with range and generally the horizontal variations of $n$ can be neglected [3]. The appearance of negative vertical gradient of the modified refractivity $M$ ($M=N+(z/a_e)10^6$, with $z$ the height above the sea surface and $a_e$ -

the Earth's radius, indicates the presence of tropospheric duct [3]. For practical purposes the average behaviour of the modified refractivity $M(z)$ is often approximated with piecewise-linear profile. On Fig. 1 are schematically presented the $M(z)$ profiles for the four duct types with essential parameters indicated.

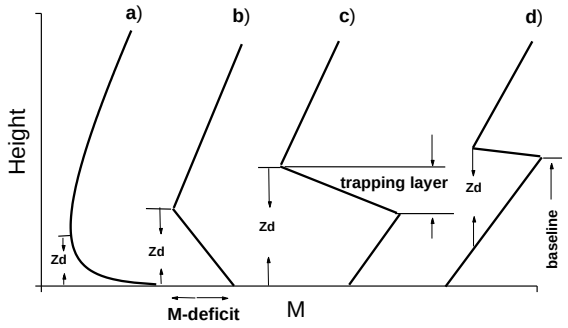


Figure 1. a) evaporation, b) surface, c) surface-based, d) elevated duct, $z_d$ – duct thickness.

The complicated maritime conditions require sophisticated propagation methods. The paraxial approximation to the wave equation, known as the parabolic equation (PE), allows correct accounting simultaneously for the strong refraction under ducting, diffraction around the Earth's curvature, reflection and scattering from the rough sea surface, and antenna pattern [4, 5]. This report studies the propagation of AIS frequencies under various tropospheric ducting and sea surface conditions with the PE method. The aim is to examine the influence of sea surface roughness on the possibility to enlarge the AIS detection range under ducting.

## 2. METHOD DESCRIPTION

In this study 2D narrow-angle forward-scatter scalar PE is used as implemented in "Advanced propagation model (APM) Computer software configuration item (CSCI) documents", Space and Naval Warfare Systems Center Tech. Doc. 3145, which allows finding a full-wave solution to the AIS signal propagation problem in terms of path loss, PL (PL in dB):

$$PL = 20\log\left(\frac{4\pi r}{\lambda}\right) - PF\,, \tag{1}$$

here $\lambda$ is the free-space wavelength, $r$ is the distance between the corresponding points and $PF$ is the propagation factor (in dB) defined as the square of the ratio of the electric field amplitude $E$ received at a given point under specific conditions to the amplitude of the electric field $E_0$ received at the same point under free-space conditions where $E$ participates with its polarization component which coincides with the polarization of $E_0$ [3]. In this study, the initial field is provided by an omni directional antenna. Equation (2) gives the expression of the $PF$ in terms of the reduced PE field, $U(x,z)$, which comes from the APM routines:

$$PF = 20\log|U(x,z)| + 10\log(r) + 10\log(\lambda). \tag{2}$$

Two international channels in the VHF maritime mobile band centered at 161.975 MHz and 162.025 MHz are allocated to the AIS. Later in the calculations the $F$=161.975 MHz is used. The examples of duct parameters have been taken from among the typical ones for the Bulgarian Black sea shore [6]. In order to preliminary assess the trapping of the AIS frequencies, well known formula for maximum wave length, $\lambda_{max}$, trapped in a duct is used [7]:

$$\lambda_{\max} = \frac{2}{3} C z_d (\Delta M)^{1/2}, \tag{3}$$

where $z_d$ is the duct thickness, $\Delta M$ is the M-deficit, see Fig. 1, and $C$=3.77x10$^{-3}$ for surface and surface-based ducts. In this report these two types of ducts have been studied: the evaporation duct, even though the most widespread over the sea, is not able to trap the AIS frequencies with its maximal height of 40 m, whereas the elevated ducts have been considered to have weak influence due to there relatively great height above the sea surface. Also, surface and surface-based ducts are less sensitive to frequency than evaporation ducts and can extend over the ocean for several hundreds of kilometers and last for multiple days.

A trans-horizon path supposes reflections from the sea surface, therefore the sea surface roughness should be accounted for. Here this is done in the framework of the "effective" reflection coefficient, $R_{eff}$, concept in which the Fresnel reflection coefficient, $R_F$, is multiplied by a roughness reduction factor $R_{rf}$ [4]:

$$R_{eff} = R_{rf} R_F \quad , \tag{4}$$

$$R_{rf} = R_{\mathrm{M-B}} = \exp\left[-2k^2\sigma_h^2 \sin^2(\alpha)\right] \mathrm{I}_0\left[2k^2\sigma_h^2 \sin^2(\alpha)\right]. \tag{5}$$

In (5) the Miller-Brown roughness reduction coefficient, $R_{\text{M-B}}$, is used [8] where $\sigma_{\text{h}}$ is the standard deviation of the sea surface height $h$, $I_0$ is the modified Bessel function of the first kind of order zero, $k$ is the free-space wave number and $\alpha$ is the local grazing angle measured with respect to the mean plane of the sea surface. The $R_{\text{M-B}}$ assumes the sea wave amplitude is Gaussian distributed with zero mean, i.e. in (5) $\sigma_{\text{h}}=h_{\text{rms}}$ where $h_{\text{rms}}$ is the root mean square deviation of the surface height. Note that the $R_{\text{M-B}}$ refers to the forward coherent reflected field (i.e. the diffuse scattered field is neglected as well as the small perturbations of the sea surface) and does not account for the shadowing and multiple scattering. The only parameter related to sea surface roughness in $R_{\text{M-B}}$ is the $h_{\text{rms}}$ which can be expressed entirely in terms of the wind speed. In (5) the quantity $2kh_{\text{rms}}\sin(\alpha)$ is the Rayleigh roughness parameter for the surface, [4], that is often used as a criterion for the degree of roughness. It is to note that when the grazing angles are very small (both ducting propagation and ship-to-ship propagation suppose small grazing angles) $R_{\text{M-B}}$ tends to 1 and thus the influence of the roughness is reduced. Nevertheless, the wavelength of AIS frequencies is about 1.85 m, i.e. it is of the same order as sea height variations in high sea states; hence, a roughness reduction factor is to be introduced to account for the reduction of the Fresnel reflection coefficient from flat surface.

There is a variety of formulae relating $h_{\text{rms}}$ to the wind speed and sea state [9, 10] depending on the sea wave spectrum used for their obtaining. In this report the relation corresponding to sea wave spectra of Pierson-Moskowitz type is applied [10]:

$$h_{rms} = 0.0051 U_{10}^2, \tag{6}$$

where $U_{10}$ is the wind speed in m/s at $h$=10 m. The dielectric characteristics of the sea surface are calculated as functions of frequency following "Propagation in Non-Ionized Media", CCIR 1986, vol.5.

## 3. RESULTS AND DISCUSSION

The first example of ducted propagation refers to a surface duct with bilinear profile (see Fig. 1 (b)) and parameters $z_d$=100 m, $\Delta M$=45 M-units, antenna height $h_a$=10 m, $F$=161.975 MHz, horizontal polarization (HOR) and smooth sea surface. It is to note that, following relation (3), this duct requires $\lambda_{max}$<1.68 m; this means that AIS frequencies ($\lambda$ around 1.85 m) will not be (completely) trapped. However, the transition from ducting to non-ducting conditions (and vice versa) for frequencies with $\lambda$ around $\lambda_{max}$ is gradual and those frequencies will have significantly extended propagation/ detection range in comparison to the standard troposphere case, see Fig. 2 and Fig. 3. On Fig. 2 is shown path loss versus range and height. Figure 3 provides the *PL* for two vertical cuts at fixed range *FixR*=20 km and *FixR*=25 km (red and black line); for comparison are given the respective cuts for standard troposphere

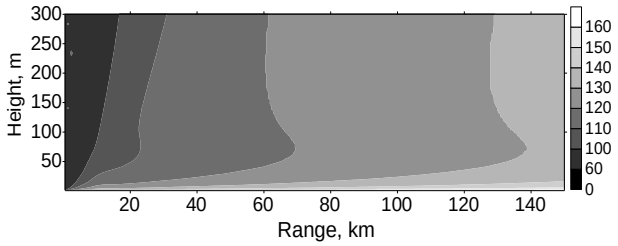


Figure 2. PL for surface duct.

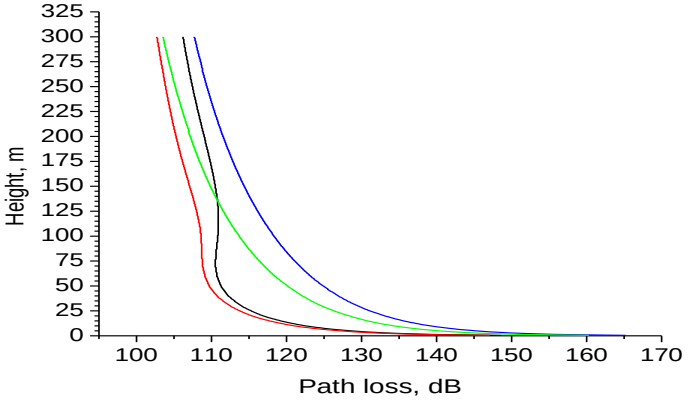


Figure 3. PL for FixR=20 km (red – surface duct, green - StanTrop) and FixR=25 km (black – surface duct, blue - StanTrop).

(StanTrop) - green and blue line. Even for these relatively short distances, 20 km and 25 km, the *PL* decrease under ducting is clearly seen, especially for the most important first

50 meters above the sea surface. With some certainty it can be expected that under similar conditions the AIS detection range will be increased.

The next four figures, Fig.4 - Fig.7, refer to a surface-based duct modelled with tri-linear profile (see Fig. 1 (c)) with parameters as follows: trapping layer base height 113 m, $z_d$=268 m, $\Delta M$=23 M-units, the slopes of the profile below and above the trapping layer correspond to the standard troposphere. The AIS frequencies are trapped by this duct. The *PL* for $h_a$=20 m and HOR is shown on Fig. 4 for standard troposphere, smooth and rough sea ($U_{10}$=9 m/s). On Fig. 5 are shown *PL* curves for fixed height *FixH*=$h_a$=20 m for the tri-linear duct and smooth sea: black curve refers to HOR, red - for VER (vertical polarization); for comparison the respective curves for StanTrop are also given (in blue and green). Clearly seen is the difference between the two polarizations. Note that close to the two *PL* peaks the *PL* under ducting exceeds that of standard troposphere. After the second peak ducting decreases significantly the *PL* but it exists a "skip zone" between 20th and 60th km, see Fig. 4 (b).

On Fig. 6 are shown *PL* curves for fixed range *FixR*=35 km (close to the first *PL* peak, see Fig. 5) for the same tri-linear duct as on Figs. 4 and 5, and HOR: the red curve refers to smooth sea, the StanTrop *PL* is given in blue, the black curve shows the influence of sea surface roughness introduced through formulas (4)-(6) for $U_{10}$=9 m/s. Figure 7 presents the *PL* for the same conditions as on Fig. 6 but only the area of interest below the first 50 meters above the sea is given: red - smooth sea; black - rough sea, $U_{10}$=9 m/s; blue - rough sea, $U_{10}$=15 m/s. As expected, the influence of ducting prevails over that of sea roughness which is negligible except in the area close to the *PL* peak. A possible reason is change of the grazing angles to the sea in the "skip zone" so that the influence of the $R_{rf}$=$R_{M\text{-}B}$ is increased. The increased roughness, $U_{10}$=15 m/s, "blurs" the *PL* pattern, see also Fig. 4 (c). The presence of "skip zones" indicates that ducting may not always be advantageous for the detection range and this may by aggravated by the sea roughness.

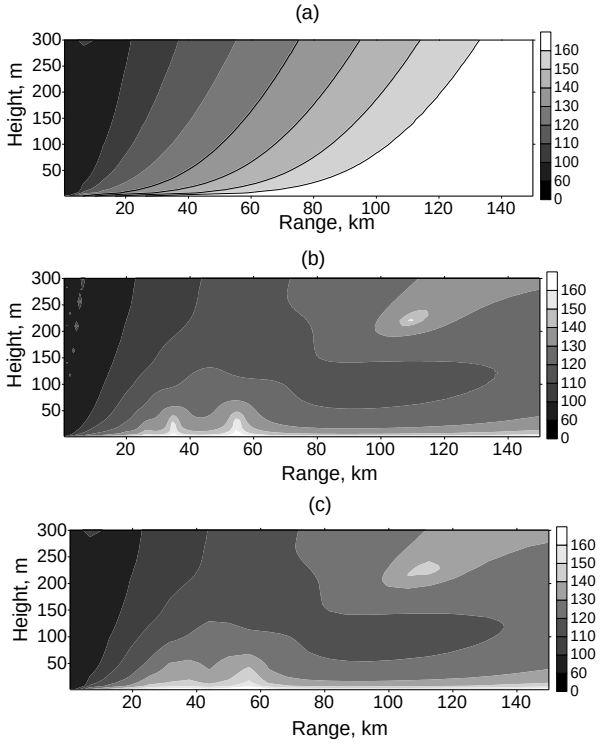


Figure 4. *PL* for $h_a$=20 m: (a) StanTrop, (b) tri-linear duct, smooth sea, (c) tri-linear duct, rough sea.

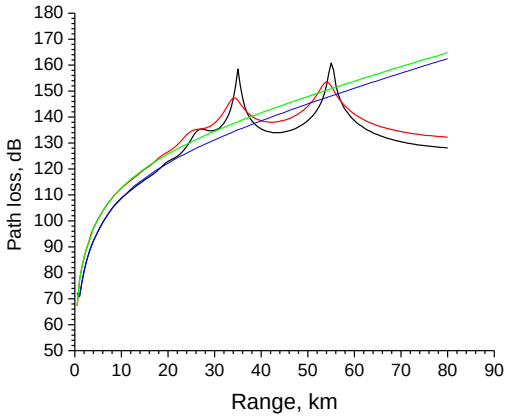


Figure 5. *PL* for *FixH*=$h_a$=20 m, tri-linear duct, smooth sea: black – HOR, red – VER, blue & green – HOR & VER for StanTrop.

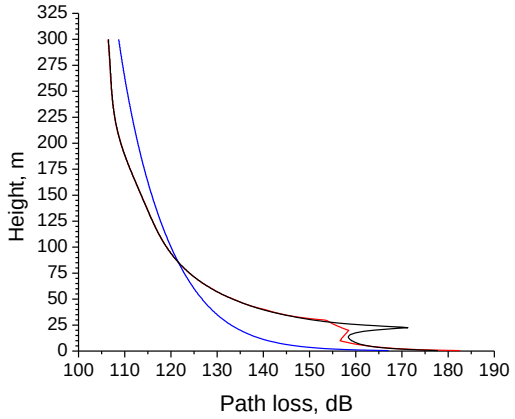


Figure 6. PL for FixR=35 km, HOR, tri-linear duct: red - smooth sea, black – rough sea, blue - StanTrop.

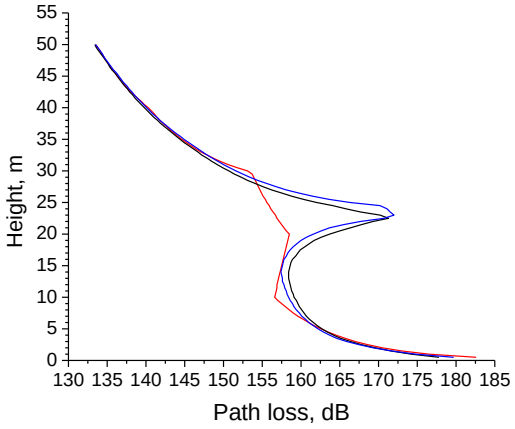


Figure 7. PL for FixR=35 km, HOR, tri-linear duct: red - smooth sea, black – rough sea, U10=9 m/s, blue - rough sea U10=15 m/s.

## 4. CONCLUSION

The results indicate that to be reliable and of practical use the extension of the detection range through ducting requires:

- a good preliminary assessment of the duct types and parameters;
- accounting for sea roughness for sea state 4 and higher (according to the scale relating wind speed to sea state [10]); even though the roughness has rather weak influence, it may increase the *PL* in the "skip zones";
- additional investigations that account for the rocking of the ship, influence of breaking waves, etc.

## 5. ACKNOWLEDGMENTS

This work was supported by the Ministry of Education and Science of Bulgaria (support for ACTRIS BG, part of the Bulgarian National Roadmap for Research Infrastructure).

## REFERENCES

[1] F. Lázaro, R. Raulefs, W. Wang et al. "VHF Data Exchange System (VDES): an enabling technology for maritime communications," CEAS Space J., vol. 11, pp. 55–63, Jul. 2019.

[2] ITU-R M.2123 “Long range detection of automatic identification system (AIS) messages under various tropospheric propagation conditions,” 2007.

[3] D. E. Kerr, (Ed.) Propagation of short radio waves. London, UK: Peter Peregrinus, 1987.

[4] M. Levy, Parabolic equation methods for electromagnetic wave propagation. UK: IEE electromagnetic waves series 45, 2000.

[5] I. Sirkova, “Brief review on PE method application to propagation channel modeling in sea environment,” CEJE, vol. 2, no. 1, pp. 19-38, 2012.

[6] I. Sirkova, “Duct occurrence and characteristics for Bulgarian Black sea shore derived from ECMWF data,” J. Atmos. Sol-Terr. Phy., vol. 135, pp. 107-117, Dec. 2015.

[7] J. D. Turton, D. A. Bennetts, and S. F. G. Farmer, "An introduction to radio ducting," Meterorolog. Mag., vol. 117, pp. 245-254, 1988.

[8] A. R. Miller, R. M. Brown, and E. Vegh, "New derivation for the rough surface reflection coefficient and for the distribution of sea-wave elevations," IEE Proc.-H, vol. 131, pp. 114–116, 1984.

[9] T. P. Leonard, I. Antipov, and K. D. Ward, "A comparison of radar sea clutter models," in Proc. Radar 2002, Edinburgh, UK, Oct. 15-17, 2002, pp. 429-433.

[10] L. B. Wetzel, “Sea clutter”, Naval Res. Lab. Report 9244, Washington, USA, 1990, 41 p.